applied sciences

MDPI

Article

Influence of Rock Mass Discontinuity on Blast-Induced Vibration Attenuation in Quarry

Chi-Han Wang [1], Yung-Chin Ding [1,*] and Fu-Hao Lee [2]

[1] Institute of Mineral Resources Engineering, National Taipei University of Technology, Taipei 106344, Taiwan; augus.wang@msa.hinet.net
[2] Taiwan Cement Corporation, Taipei 104, Taiwan
* Correspondence: ycding@ntut.edu.tw; Tel.: +886-2-27712171 (ext. 2733)

Abstract

This study investigates the influence of rock mass discontinuities on blast-induced ground vibration attenuation in a marble quarry in eastern Taiwan. A total of 53 blasts and 106 vibration records were collected and analyzed using image-based rock mass characterization with WipFrag (Version 4) software. Discontinuity conditions were quantified through the joint factor (JF), defined by the median size (D50) and maximum size (D100) from cumulative size distribution curves. The PPV (peak particle velocity) data were fitted using the USBM, Sadovsky, and a modified Simangunsong equation incorporating a discontinuity correction factor. The modified Simangunsong model yielded the highest correlation (R^2 = 0.8632), followed by the Sadovsky (R^2 = 0.8067) and USBM (R^2 = 0.7674) equations, indicating improved in-sample fitting performance when discontinuity effects are included. The results show that explicitly considering discontinuity effects enhances the reliability of PPV estimates for the studied site and that highly fractured rock masses with smaller block sizes result in greater vibration attenuation. The study demonstrates that a practical approach to quantify discontinuities through image analysis and embedding them into empirical PPV attenuation models can be used to refine quarry blasting design for vibration control purposes.

Keywords: quarry blasting; peak particle velocity; ground vibration control; rock mass discontinuities; image-based fragmentation

1. Introduction

Blasting is the most widely used production operation in quarries, with its effectiveness having a direct impact on subsequent operations including loading, hauling, and crushing. Rock fragmentation serves as a principal metric for evaluating blasting efficiency [1]. In recent years, digital image-based techniques have been increasingly applied for quantitative fragmentation analysis and structural characterization of bench faces, providing efficient and non-contact assessment methods [2,3].

However, blasting operations in quarries generate ground vibrations that may propagate to surrounding environments, potentially affecting nearby residential areas, buildings, and infrastructure. Excessive blast-induced vibration can lead to structural damage and environmental disturbance; therefore, accurate estimation and management, and effective control of blasting vibration are important issues in quarry engineering. Peak particle velocity (PPV) is commonly used as the primary indicator for evaluating and managing blasting vibration impacts.

Check for updates

Academic Editor: Gino Iannace

Received: 10 March 2026
Revised: 13 April 2026
Accepted: 17 April 2026
Published: 20 April 2026

Copyright: © 2026 by the authors. Licensee MDPI, Basel, Switzerland. This article is an open access article distributed under the terms and conditions of the Creative Commons Attribution (CC BY) license.

In this study, field blasting parameters, monitored PPV data, and image-based fragmentation information of the quarry bench rock mass were integrated to establish quantitative relationships between geological conditions and blasting vibration responses. Rock mass discontinuities were characterized by ranked from pre-blast bench faces, which were then to be incorporated into regression analysis, enabling the determination of site-specific empirical constants (K and α) that reflect the influence of local geology.

Both the conventional USBM empirical model [4] and the modified Simangunsong equation incorporating a joint factor (Mod-JF) [5] were evaluated and compared to assessing their applicability under the site's specific geological conditions. By embedding these discontinuity-derived parameters into empirical attenuation equations, the study demonstrates improved fitting performance and reduced residual errors in PPV for the investigated dataset and highlights the significant role of rock mass discontinuities in vibration attenuation.

1.1. Empirical PPV Models and Their Limitations

Ground vibrations induced by blasting are commonly evaluated using peak particle velocity (PPV). PPV has long been widely adopted in quarry engineering and vibration control studies as a standard indicator for assessing blast-induced ground motion. Among the various empirical equations developed to predict PPV, the (1) United States Bureau of Mines (USBM) Equation [4] and (2) the Sadovsky Equation [6] are the most commonly used:

The USBM equation is defined as follows:

$$V = K\left(\frac{R}{\sqrt{Q}}\right)^{\alpha} \quad (1)$$

The Sadovsky equation is given by:

$$V = K\left(\frac{\sqrt[3]{Q}}{R}\right)^{\alpha} \quad (2)$$

where V (mm/s) is the PPV, R (m) is the distance from the blast source, and Q (kg) is the maximum instantaneous charge per delay. The parameters K and α are empirical constants obtained through regression analysis. The constant K is generally regarded as a site-dependent coefficient reflecting rock mass conditions and blasting characteristics, whereas α represents the attenuation exponent associated with geological conditions and wave propagation characteristics, indicating the rate at which vibration amplitude decays with distance.

However, rock mass discontinuities—such as joints, bedding planes, and fractures—can alter the propagation path of stress waves and influence vibration attenuation behavior. Aloui and Abbes demonstrated that increases in the cumulated aperture of fractures (CA) and cumulated fracturing intensity (IF) enhance wave attenuation in fractured rock masses, thereby reducing peak particle velocity (PPV) [7]. Consequently, the empirical constants K and α derived from conventional attenuation equations implicitly incorporate the combined effects of rock mass structural characteristics, yet without explicitly quantifying discontinuity parameters. Therefore, these empirical equations, once established, cannot be easily applied to blasting sites that have high rock mass structure variation.

1.2. Influence of Rock Mass Discontinuities on Blasting Performance

The orientation (strike and dip) and spacing of rock mass discontinuities, together with rock mass strength, may alter the propagation path and attenuation mechanisms of blast-induced stress waves, thereby affecting fragmentation performance [8–10].

Worsey et al. [11] reported that the effectiveness of controlled blasting (pre-splitting) is strongly governed by the angle between the designed presplit line and pre-existing discontinuities. The performance of the controlled blasting deteriorates when this angle is <60° and becomes essentially indistinguishable from conventional blasting when it is <15° [11]. Such joint geometry characteristics, including orientation and distribution, significantly influence stress wave transmission and reflection at discontinuity interfaces, thereby modifying stress wave paths and energy dissipation patterns during blasting [12,13].

Blasting performance is strongly influenced by structural orientation [14]. The relationship between the direction of structural orientation and the direction of blasting boreholes can be broadly classified into three types: (a) blasting with the dip, (b) blasting against the dip, and (c) blasting along the strike. With-the-dip blasting tends to increase backbreak and displacement while reducing toe damage, whereas against-the-dip blasting produces the opposite trend. Structures perpendicular to the slope strike may generate serrated bench profiles [14].

These observations suggest that structural orientation plays a key role in stress-wave transmission and energy distribution, thereby influencing fracture development and bench stability [15,16].

Lyana et al. investigated the influence of geological conditions on rock fragmentation in a marble quarry in Simpang Pulai, Perak, Malaysia [17]. Fieldwork included detailed geological mapping and RMR assessment prior to blasting, with geotechnical parameters such as discontinuity length, spacing, weathering, infilling, and intact rock strength obtained through rock mass classification and uniaxial compressive strength testing. Post-blast muck pile images were analyzed using WipFrag (Version 4) software to quantify fragmentation, and the results demonstrated that rock mass strength and discontinuity properties significantly affect blast fragmentation outcomes.

Although geological discontinuities are widely recognized to influence blasting performance and fragmentation, their effects are seldom explicitly incorporated into empirical PPV attenuation models [18]. Conventional equations primarily rely on charge weight and distance, leaving structural influences implicitly embedded within regression constants. As a result, the predictive capability of traditional models under varying geological conditions remains limited.

This study aims to quantify rock mass discontinuities using image-based analysis and incorporate the derived parameters into empirical PPV attenuation equations. Field monitored PPV data, and image-based fragmentation information were integrated to establish quantitative relationships between geological conditions and blasting vibration responses. Rock mass discontinuities characterized from pre-blast bench faces were incorporated into regression analysis, enabling the determination of site-specific empirical constants (K and α) that reflect the influence of local geology. By comparing the conventional USBM and Sadovsky models with a modified equation incorporating a joint factor, the influence of discontinuities on vibration attenuation behavior can be systematically evaluated in a more accurate manner.

2. Methods

Figure 1 shows the experimental procedure conducted in this study. Before quarry bench blasting, blasting design parameters such as charge weight, initiation position, spacing, burden, and delay timing were collected. Vibration sensors (Instantel MiniMate Plus, Ottawa, ON, Canada) were set up and positioned. Digital images of benches to be blasted were taken before blasting. These photographs were analyzed to obtain the particle size distribution curve, which was then to be used to determine the Joint Factor of the quarry bench. After blasting, PPV values were measured. Finally, the blasting

vibration data obtained were subjected to regression analysis using the conventional USBM, Sadovsky equation, and the JF incorporated modified Simangunsong equation.

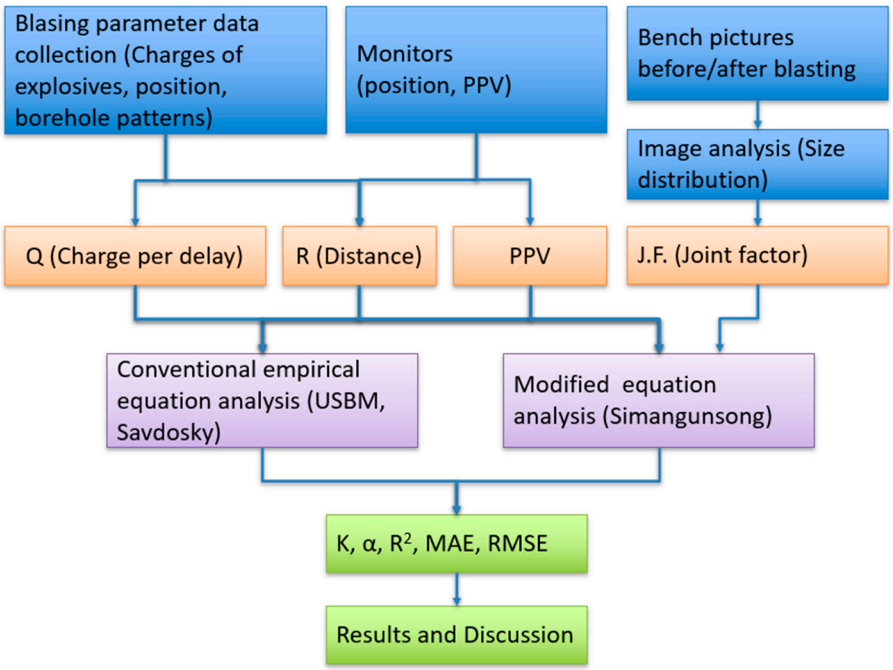


Figure 1. Experimental procedure flowchart.

The coefficient of determination (R^2) was used to evaluate the goodness of fit for each regression model. A higher R^2 value indicates better model performance in explaining the variance in the observed PPV data. Additionally, the mean absolute error (MAE) and root mean square error (RMSE) were calculated to quantify the in-sample fitting error of the models.

2.1. Site Description and Field Measurement

This blasting vibration measurements were conducted at a cement raw material quarry in Hualien County, eastern Taiwan. The marble mined at this quarry has a compressive strength ranging from 80 to 90 MPa, cohesion from 15 to 18.5 MPa, and an internal friction angle from 45 to 51°. The thickness of the marble layer is about 500 m, with the main strike of N30E and a dip angle of 25S. The rock mass exhibits well-developed joints. The blasting design parameters of the quarry are shown in Table 1.

Table 1. Blasting design parameters.

Spacing × Burden	4.5 m × 2.8 m
Borehole Diameter	105 mm
Borehole Angle and Depth	75°/11 m
Bench Height	10.0 m
Delay Time	25 ms between holes 67 ms between rows
Explosive types	Cartridge Emulsion & ANFO

The vibration monitors were installed behind or to the side of the blasting site at approximately the same elevation level, as shown in Figure 2. Two monitors were positioned in the same general direction, approximately aligned in a straight line with the blast

vibration source. The detonation point, monitor positions, and the distances between them were surveyed and recorded prior to each blast.

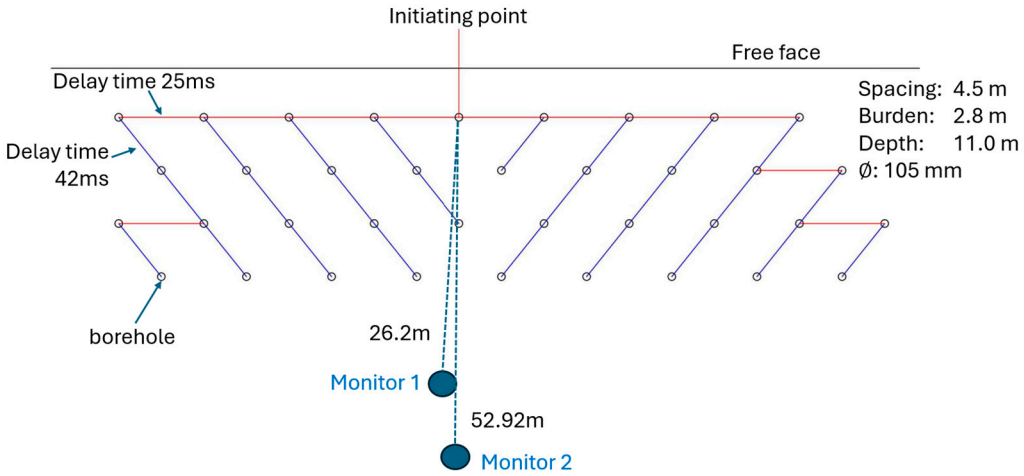


Figure 2. Layout of blasting pattern and monitoring positions.

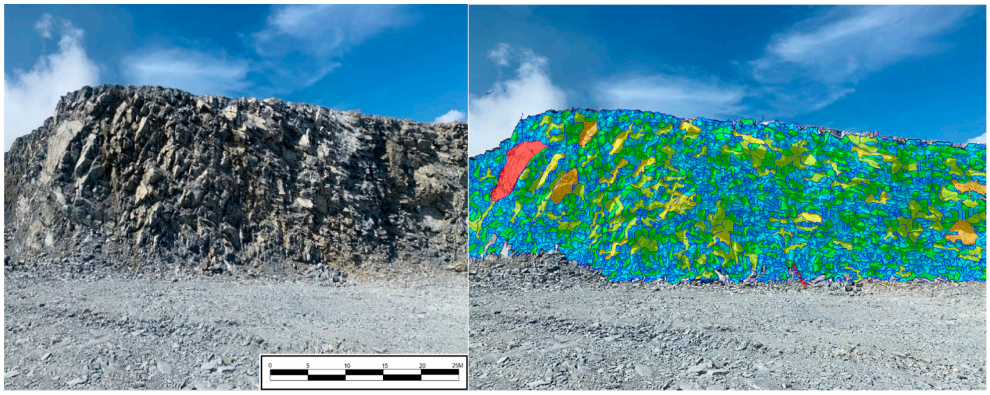
Each blasting operation adopted the same design parameters, including spacing, burden, borehole depth, and borehole angle. The instantaneous charge weight Q (kg), and the distance between the blast source and each monitor R (m), were recorded for every blast. For each of the 53 production blasts, PPV was measured at two monitoring locations, yielding a total of 106 PPV records. The resulting dataset was then used to calibrate the USBM, Sadovsky, and modified Simangunsong empirical equations. Because the two PPV measurements obtained for each blast correspond to the same blasting event, they may not be statistically independent. Therefore, the regression results should be interpreted with caution, as intra-blast correlation may lead to optimistic estimates of goodness-of-fit and error statistics.

2.2. Image Analysis and Quantitative Characterization of Discontinuities

Natural rock masses typically contain numerous discontinuities, including bedding planes, joints, and faults, which act as barriers to vibration waves. When vibration waves encounter discontinuities with stiffness contrast or gaps, part of the wave energy is reflected, refracted or dissipated, affecting the attenuation and PPV recorded by the monitors or experienced by nearby residents. To investigate the influence of these discontinuities on blast-induced vibrations, it is necessary to quantify the degree of fracturing of the rock mass. In this study, WipFrag image analysis software was used for this purpose.

Digital images of the quarry bench were taken before blasting, as shown in Figure 3. Through image analysis, the degree of fracturing of the bench before blasting can be quantified and classified into several rankings. To ensure consistency of the analysis, all photographs were captured using the same camera model and lens, with the camera positioned approximately 15 to 30 m from the bench face. It is recommended that photographs be taken under similar lighting conditions, avoiding situations where the sun is directly in front of the camera or when the bench face is heavily shadowed.

Each photograph should include a scale reference, such as an object or marker of known size or distance, or by using the known height of the bench as a scale. This reference is then used within the software to calibrate the pixel-to-length conversion factor, allowing direct comparability of fragment size measurements across different blasting operations.



(**a**) (**b**)

Figure 3. (**a**) Photograph of the bench face used on image analysis. (**b**) Rock boundary analyzed by WipFrag software. In the image analysis, red denotes the coarsest fragments, yellow the next coarsest, green finer fragments, and blue the finest fragments.

Afterward, each bench photograph was imported into WipFrag and calibrated using a defined scale reference. Edge detection algorithms were subsequently applied to delineate visible block boundaries and discontinuity traces on the bench surface. After automatic delineation, any incorrectly identified edges were manually refined. The segmented blocks were then analyzed to determine their equivalent particle sizes based on projected area and an assumed shape factor. A cumulative particle size distribution curve was finally generated by WipFrag (Figure 4), illustrating the pre-blast rock fragment size distribution.

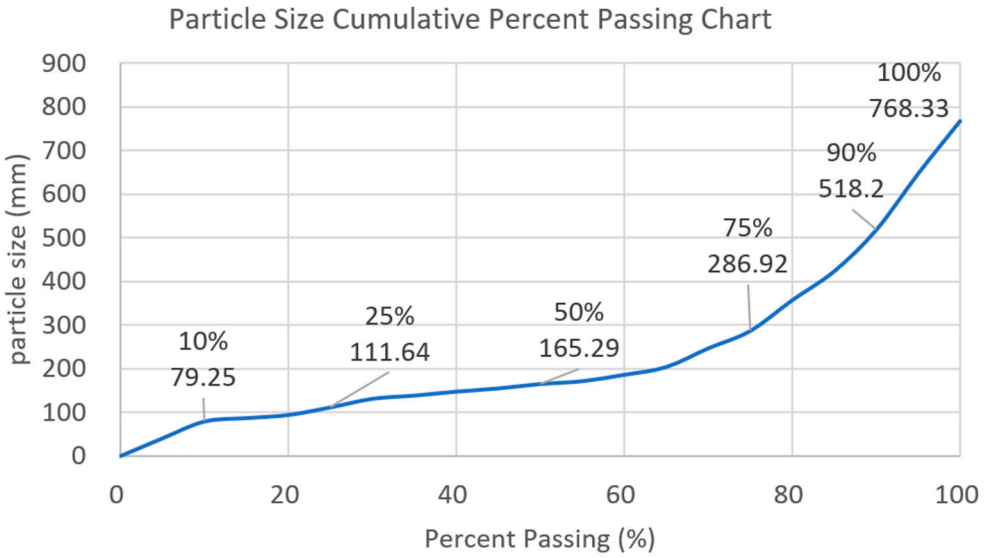


Figure 4. Cumulative particle size distribution curve of rock mass from image analysis of Figure 3.

The advantage of employing image analysis software in this study lies in its capability for automated computation and the provision of relatively objective analytical data, particularly in quantifying the degree of fracturing and discontinuity within the rock mass prior to blasting.

Figure 5 presents a bench photograph from another blast, while Figure 6 illustrates the corresponding particle size distribution curve of the bench. A comparison between Figures 4 and 6 indicates that the bench shown in Figure 5 exhibits fewer discontinuities and consequently larger rock blocks than the rock mass depicted in Figure 3. The maximum particle size (D100) reaches 768.33 mm in Figure 3, whereas in Figure 5 it increases significantly to 3536.49 mm.

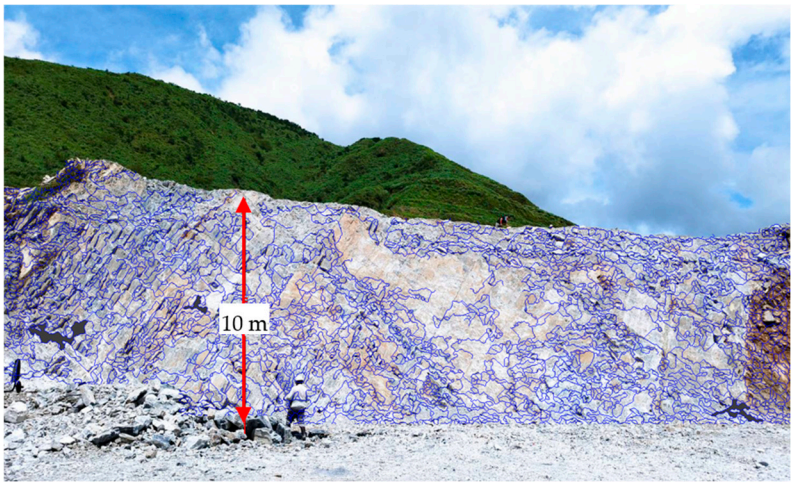


Figure 5. Photograph and image analysis of bench with lower joint frequency before blasting.

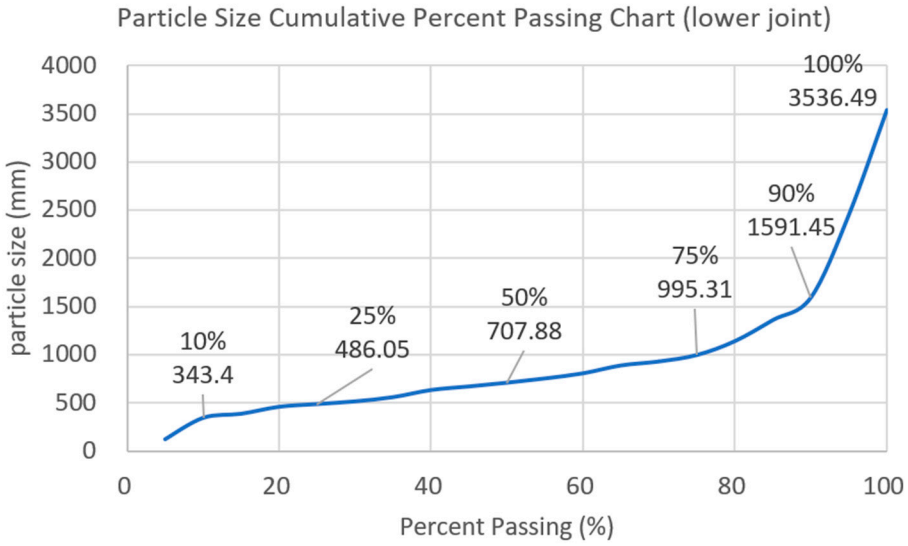


Figure 6. Cumulative particle size distribution of bench rock mass from image analysis of Figure 5.

For quarrying operations, numerous discontinuities such as bedding planes and joints commonly exist in the quarry rock mass. These discontinuities induce a damping effect as the blast-induced vibration waves propagate through the rock mass. When the discontinuity spacing is relatively small, or when interlayers or gaps are present, the attenuation of the vibration wave increases correspondingly. By using photographic and image analysis techniques, the particle size distribution curve of the rock mass before blasting can be quantitatively defined.

This quantified quarry bench fracturing data were then incorporated into empirical blasting vibration equations. As shown in Figures 4 and 6, the particle size corresponding to the 50% passing size (D50) and the maximum size (D100) in the cumulative size distribution curve were used for bench fracturing classification. Based on their size ranges, D50 and D100 were discretized into a scale of 1 to 5, representing the median and maximum block sizes, respectively. The joint factor components (JF1 for D50 and JF2 for D100) were defined according to the grading scheme in Table 2. The average of these two grades was then taken as the discontinuity coefficient (JF) used in the modified Simangunsong equation.

Table 2. Quantitative index of joint coefficient.

D_{50} (mm)	JF_1	D_{100} (mm)	JF_2
$1200 \leqq D_{50}$	1	$4000 \leqq D_{100}$	1
$900 \leqq D_{50} < 1200$	2	$3000 \leqq D_{100} < 4000$	2
$600 \leqq D_{50} < 900$	3	$2000 \leqq D_{100} < 3000$	3
$300 \leqq D_{50} < 600$	4	$1000 \leqq D_{100} < 2000$	4
$0 \leqq D_{50} < 300$	5	$0 \leqq D_{100} < 1000$	5
$JF = (JF_1 + JF_2)/2 \approx 1.0\sim5.0$			

In this study, D50 is used to represent the characteristic or average block size of the bench, reflecting the overall degree of fracturing in the rock mass, whereas D100 reflects the maximum intact block size that can still be identified on the bench face. Together, these two parameters capture both the typical block size and the presence of larger, relatively intact blocks, which jointly influence the scattering, reflection, and energy dissipation of blast-induced vibration waves. The discretization of the continuous D50 and D100 values into five classes was based on engineering judgement and typical fragmentation ranges observed at the site, with the aim of providing a simple and practical index for routine use in quarry operations. Accordingly, JF is adopted as a simplified yet physically meaningful indicator of the discontinuity condition for use in empirical vibration attenuation equations. It should be noted that the proposed JF is an image-derived proxy based on particle-size descriptors obtained from bench photographs, rather than a full geomechanical characterization of rock mass discontinuities. Accordingly, JF mainly reflects the apparent degree of surface fracturing and block-size distribution visible on the bench face. Parameters such as discontinuity orientation, persistence, aperture, infilling, spacing variability, and joint-set geometry were not explicitly included in the present formulation and may also influence blast-induced vibration attenuation.

2.3. Empirical Equations and Regression Analysis

The factors influencing vibration waves are highly complex, including the geological properties of the rock mass, and blasting design parameters (such as explosive type, charge weight, hole depth, sub-drilling, spacing, burden, delay time. . .etc.). Many researchers have proposed empirical equations for estimating vibration levels, all of which require regression analysis based on field measurements. The aim is to derive site-specific that allow refinement of these empirical equations and improve their suitability for local geological and blasting conditions.

The instantaneous charge weight Q (kg) and blasting distance R (m) are combined as the scale distance (SD), defined as SD (USBM) = $R/\sqrt{Q}$ and SD (Sadovsky) = $(\sqrt[3]{Q}/R)$. Taking the logarithm of both sides of the equation yields a linear relation, allowing regression analysis or least squares fitting to determine the attenuation parameters K and α based on the measured PPV, charge weight, and distance.

$$\log V = \log K + SD^{\alpha} \quad (3)$$

Both USBM and Sadovsky empirical equations require a sufficient number of data points to derive localized geological and attenuation coefficients K and α. However, since rock mass discontinuities may vary between blasting events, the empirical USBM and Sadovsky models cannot adequately account for their influence on vibration wave propagation.

To incorporate the effects of discontinuities, this study adopted the modified empirical equation proposed by Simangunsong [5], as shown in Equation (4), where the discontinuity rating value JF was included in the regression analysis.

$$PPV = K(SD_{JF})^{-\alpha} = K\left\{[1 + \log(1 + JF \times R)]\frac{R}{\sqrt{Q}}\right\}^{-\alpha} \quad (4)$$

where JF is the correction factor representing the influence of rock mass discontinuities. Using this approach, the attenuation constants K and α were similarly obtained. In this formulation, the discontinuity-related correction term should be regarded as an empirical adjustment introduced to capture part of the effect of bench fracturing conditions on vibration attenuation. Its role is phenomenological rather than strictly mechanistic, and further work is needed to assess its physical interpretation and the most appropriate mathematical form. In particular, the interaction between JF and distance was adopted here as a practical regression-based term for site-specific calibration and should not be interpreted as a universally validated constitutive relationship. The predicted vibration values from the modified equation were subsequently compared with results obtained using the USBM and Sadovsky methods, as well as with field measurements.

3. Results

3.1. Regression Results of the USBM Method

In this study, a total of 106 vibration monitoring records were collected from 53 blasting events. Through least squares regression, the parameters K and α of the USBM empirical equation were determined.

After conducting regression analysis of the 106 datasets, the K value of 1061.207 and the α value of -1.9831 in the USBM equation were determined. The coefficient of determination R^2 was calculated as 0.7674, as shown in Figure 7. The PPV estimate equation based on the USBM method is shown in Equation (5).

$$PPV = 1061.207\left(\frac{R}{\sqrt{Q}}\right)^{-1.9831} \quad (5)$$

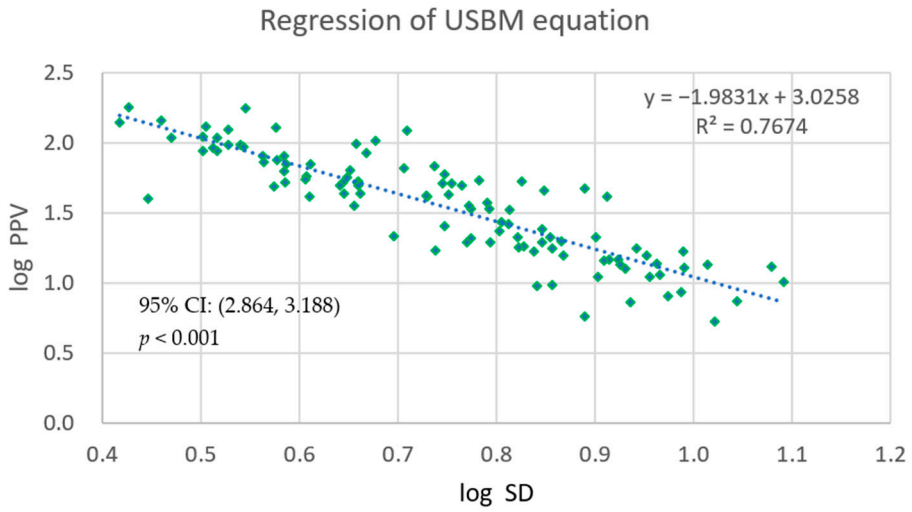


Figure 7. Regression analysis of the USBM equation.

Similarly, the 106 data points were also subjected to regression analysis using the Sadovsky equation. The resulting K value was 5671.527, the α value was 2.0263, and the

coefficient of determination R^2 was 0.8067, as shown in Figure 8. The PPV estimate equation based on the Sadovsky method is given in Equation (6).

$$PPV = 5671.527\left(\frac{\sqrt[3]{Q}}{R}\right)^{2.0263} \quad (6)$$

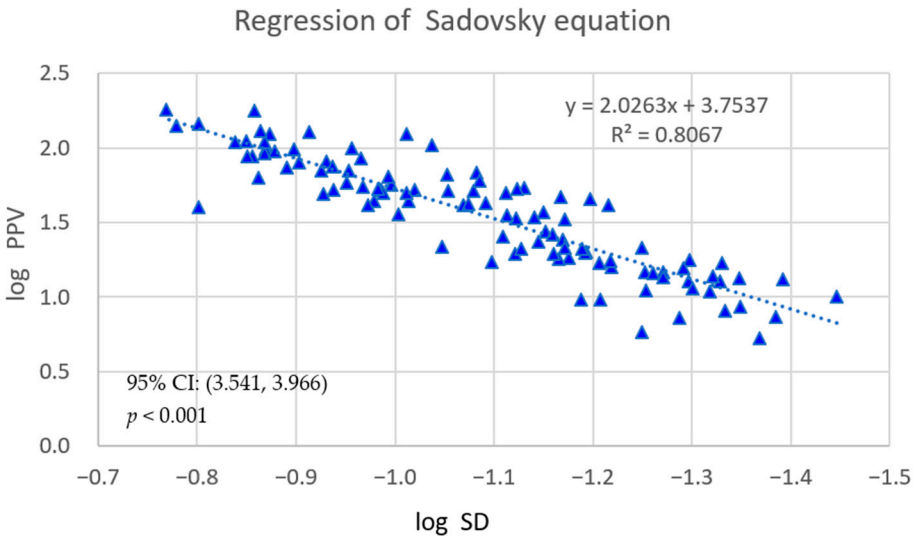


Figure 8. Regression analysis of the Sadovsky equation.

Before incorporating the modified parameter for discontinuities, among the two commonly used conventional equations, the Sadovsky equation aligns more closely with the field measurements, exhibiting a higher R^2 value (0.8067), lower mean absolute error (MAE) of 12.22 mm/s, and lower root mean square error (RMSE) of 20.04 mm/s. In comparison, the USBM method has an R^2 value of 0.7674, MAE of 13.06 mm/s, and RMSE of 21.61 mm/s. The higher RMSE is mainly due to several outlier values in the regression analysis dataset, which result in larger residuals. This is probably because the K and α values determined in the USBM equation cannot fully represent the geological conditions of the bench being blasted, or the higher geological structure variation among those blasting benches under investigation.

3.2. Regression Analysis in Simangunsong Modified Equation

In order to further define the fracturing characteristics of the quarry bench before blasting, the digital images of the quarry benches were taken and analyzed using WipFrag software. Based upon the particle size distribution curves, the 50% cumulative passing size D_{50} and the maximum particle size D_{100} were used to rank the JF (join factor) ranging from 1.0 to 5.0 as shown in Table 2. This ranking was then assigned to each blasting bench rock mass. The resultant bench JF rankings prior to the 53 blasting events and their corresponding discontinuity index values are listed in Table 3.

Table 3. Discontinuity JF ranking from 53 blast bench photograph image analysis.

No.	D_{50}	D_{100}	JF_1	JF_2	JF	No.	D_{50}	D_{100}	JF_1	JF_2	JF	No.	D_{50}	D_{100}	JF_1	JF_2	JF
1	1304	3704	1	2	1.5	19	359	1270	4	4	4	37	457	2393	4	3	3.5
2	389	1179	4	4	4	20	1147	4327	2	1	1.5	38	552	2406	4	3	3.5
3	688	2906	3	3	3	21	754	2689	3	3	3	39	702	3543	3	2	2.5
4	1047	3575	2	2	2	22	894	3799	3	2	2.5	40	828	3268	3	2	2.5
5	1389	4656	1	1	1	23	691	2229	3	3	3	41	1259	4125	1	1	1
6	910	3136	2	2	2	24	998	2534	2	3	2.5	42	428	2268	4	3	3.5

Table 3. *Cont.*

No.	D_{50}	D_{100}	JF_1	JF_2	JF	No.	D_{50}	D_{100}	JF_1	JF_2	JF	No.	D_{50}	D_{100}	JF_1	JF_2	JF
7	623	2385	3	3	3	25	818	2860	3	3	3	43	352	1095	4	4	4
8	255	1857	5	4	4.5	26	1082	3812	2	2	2	44	1741	4053	1	1	1
9	1048	3914	2	2	2	27	934	3658	2	2	2	45	1287	3728	1	2	1.5
10	226	672	5	5	5	28	260	1903	5	4	4.5	46	942	2909	2	3	2.5
11	1388	4086	1	1	1	29	1101	4362	2	1	1.5	47	1491	3815	1	2	1.5
12	1161	3379	2	2	2	30	573	2584	4	3	3.5	48	894	3799	3	2	2.5
13	1054	3745	2	2	2	31	523	2351	4	3	3.5	49	787	2172	3	3	3
14	1049	3854	2	2	2	32	1133	4246	2	1	1.5	50	468	2143	4	3	3.5
15	246	796	5	5	5	33	1246	3535	1	2	1.5	51	804	3203	3	2	2.5
16	260	1903	5	4	4.5	34	1332	5393	1	1	1	52	215	1014	5	4	4.5
17	288	877	5	5	5	35	708	3536	3	2	2.5	53	186	889	5	5	5
18	305	1856	4	4	4	36	165	768	5	5	5						

The JF, Q, and R values from each blasting event were substituted into the Simangunsong empirical equation for regression analysis. The obtained parameters for the Simangunsong equation were K = 6916.717, and α= −1.8388, as shown in Equation (7) and Figure 9.

$$\mathrm{PPV} = 6916.717\left\{[1+\log(1+\mathrm{JF}\ \times\ \mathrm{R})]\frac{\mathrm{R}}{\sqrt{\mathrm{Q}}}\right\}^{-1.8388} \quad (7)$$

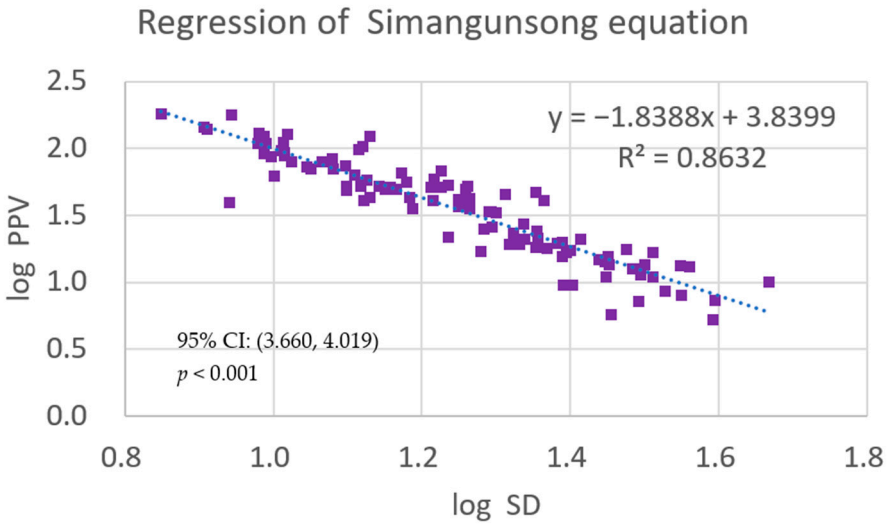


Figure 9. Regression analysis of the discontinuity modified Simangunsong equation.

According to the regression analysis results, the K and α values calculated for the USBM, Sadovsky, and Simangunsong equations are summarized in Table 4. The substantial improvement in fitting performance achieved by the modified Simangunsong equation confirms that rock mass discontinuities play a critical role in blast vibration attenuation. The Simangunsong equation achieved the highest R^2 value and the lowest error. This demonstrates that adding the discontinuity correction parameter allows the regression empirical equation to better reflect actual geological conditions at the site and provides an estimate of blast-induced vibrations that more closely matches the field measurement data. However, because model calibration and evaluation were performed on the same dataset, these results should be interpreted as an improvement in in-sample fit rather than as definitive evidence of superior predictive performance.

Table 4. Comparison of Three Empirical Regression Equations for Predicting Blast-Induced Vibrations.

Parameters	USBM	Sadovsky	Simangunsong
K	1061.207	5671.517	6916.717
α	−1.9831	2.0263	−1.8388
R^2	0.7674	0.8067	0.8632
MAE	13.06 mm/s	12.22 mm/s	9.90 mm/s
RMSE	21.61 mm/s	20.04 mm/s	16.78 mm/s

The value of the discontinuity correction parameter can be derived using field photos and image analysis software. By measuring the passing particle sizes D50 and D100, the corresponding parameter score can be obtained and directly substituted into the equation for regression analysis, thereby avoiding uncertainties caused by subjective human judgment.

By comparing the conventional empirical equations used in this study, Sadovsky demonstrates higher reliability and lower error values than those of USBM. The main difference between the two equations lies in the treatment of the scale distance, where Sadovsky uses the cube root of Q, while USBM adopts the square root of Q. In this case, the higher reliability and lower error of the Sadovsky equation may be attributed to its blasting design and/or the geological conditions being closer to the quarry being investigated in this study.

Additionally, in order to understand the error values of the three empirical equations under different JF coefficients, this study organizes the error values for various JF grades as shown in Table 5 and Figure 10.

Table 5. Summary of fitting errors of USBM, Sadovsky, and Simangunsong equations.

J.F.	USBM-MAE	USBM-RMSE	Sadovsky-MAE	Sadovsky-RMSE	Simangunsong-MAE	Simangunsong-RMSE
1.0	37.70	46.64	33.77	41.44	25.29	32.04
1.5	15.42	21.17	16.63	21.84	12.55	17.53
2.0	12.00	17.67	10.70	15.08	10.47	14.61
2.5	5.61	8.25	5.94	9.39	4.98	7.71
3.0	4.33	5.59	5.12	7.55	4.13	6.20
3.5	6.41	8.84	4.83	6.85	4.23	6.49
4.0	21.96 * 11.05	36.65 * 12.41	19.61 * 8.85	34.84 * 9.99	16.85 * 6.50	32.33 * 7.43
4.5	9.22	10.78	7.51	8.81	5.24	6.94
5.0	13.09	15.41	12.18	14.44	9.66	10.89

Note: All error values are presented in consistent units (mm/s). * indicates the error value after removing one outlier from the dataset.

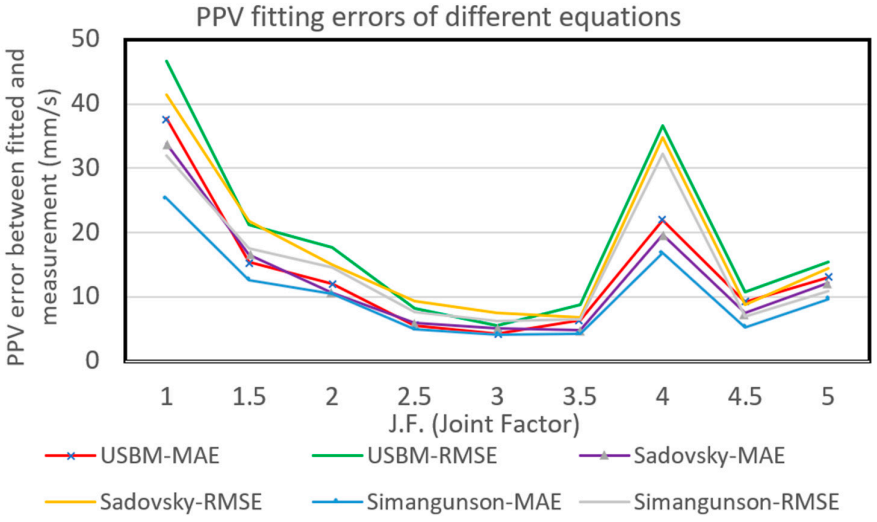


Figure 10. Summary of PPV fitting errors of the USBM, Sadovsky, and Simangunsong equations.

For each JF value, the Simangunsong equation exhibits lower MAE and RMSE than the USBM and Sadovsky models, indicating the smallest overall fitting error and thus the most consistent performance on the available dataset. Between USBM and Sadovsky, the MAE and RMSE of Sadovsky model are generally slightly lower than those of USBM, suggesting a modest improvement in performance of fit. However, these differences are not as pronounced as those observed for the Simangunsong model, which incorporates site-specific joint factors derived from image analysis.

As shown in Table 5, when the JF range is between 2.5 and 3.5, the fitting errors of the three equations are relatively low. In contrast, when J.F. = 4, the errors increase markedly. Upon re-examining the original field measurement data, it was found that one outlier is present in the dataset for J.F. = 4 (Q = 135 kg, R = 32.45 m, PPV = 40.1 mm/s), where the measured PPV value is considerably lower than other records with similar scale distances. This can probably be attributed to the presence of a joint-intensive or weathered interlayer zone at that bench level, partial waveform interference caused by blasting delays between adjacent boreholes, or potential measurement errors. After excluding this data point, the error curves of the three empirical equations (as shown in Figure 11) become noticeably smoother. When the J.F. value is low (1.0–2.0), it indicates that the bench contains fewer discontinuities and larger rock fragments, which is associated with relatively higher error values, with the largest discrepancy observed at JF = 1.0.

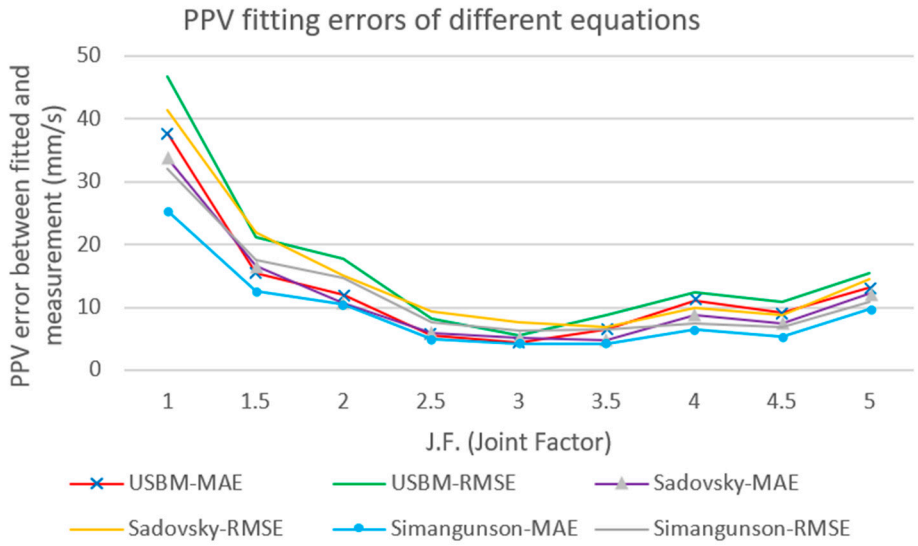


Figure 11. PPV fitting errors of the USBM, Sadovsky, and Simangunsong equations after removing the outlier.

4. Discussion

This study investigated the influence of rock mass discontinuities on the propagation of blast-induced vibrations in a thick-bedded marble quarry located in eastern Taiwan. A total of 53 production blasts, generating 106 Peak Particle Velocity (PPV) records, were analyzed using both the conventional USBM and Sadovsky empirical equations, as well as the modified Simangunsong equation that incorporates a joint factor (JF) derived from image-based fragmentation characteristics.

Regression analysis using the USBM and Sadovsky methods yielded site-specific attenuation coefficients with R^2 values of 0.7674 and 0.8067, respectively, indicating a limited yet reasonable ability to capture PPV variation solely through maximum instantaneous charge and distance. When JF, representing the combined influence of median particle size D50 and maximum particle size D100, was incorporated into the Simangunsong equation, the regression results improved to R^2 = 0.8632. This improvement indicates that explicitly

accounting for rock mass discontinuity characteristics can markedly enhance the fitting performance empirical PPV models for the studied site.

Further analysis revealed that higher discontinuity frequencies and smaller rock block sizes, corresponding to higher JF values, are associated with stronger attenuation of blast-induced vibration waves during propagation. Conversely, when JF values are low (1.0–2.0), indicating fewer discontinuities and larger block sizes, higher fitting errors are observed.

However, when JF = 4, an apparent increase in error was identified across all three empirical equations. Upon re-examining the field data, one outlier was found (Q = 135 kg, R = 32.45 m, PPV = 40.1 mm/s) whose PPV was abnormally low compared to other data points with similar scale distances. Possible explanations include (i) the presence of a joint-intensive or weathered interlayer zone, (ii) partial waveform interference due to blast delay timing, or (iii) measurement error. When this data point was excluded, the error distributions of the three empirical models became noticeably smoother and more consistent, suggesting that local geological anomalies or measurement uncertainties can significantly influence regression performance.

The application of image analysis for assessing pre-blast bench conditions proves to be an effective and relatively objective means of quantifying discontinuity characteristics. Unlike conventional joint surveys that are time-consuming and subjective, the proposed image-based approach allows for rapid and repeatable evaluation, facilitating its incorporation into routine blast design workflows. The image-based approach allows for rapid and repeatable evaluation, facilitating its incorporation into routine blast design workflows. The joint factor (JF) provides a practical, data-driven index for representing geological variability in empirical blast vibration models. Because local geological and geomechanical conditions may vary markedly even within apparently similar settings, site-specific characterization remains essential when calibrating empirical models for vibration response [19].

Overall, the study confirms that empirical vibration models should incorporate rock mass discontinuity characteristics rather than relying solely on charge weight and distance. This is particularly important for highly jointed rock masses such as marble deposits used for cement production. The proposed approach of this study provides a useful framework for site-specific blast design and vibration control, contributing to improved operational efficiency and compliance with vibration-related safety and environmental standards.

5. Conclusions

This study suggests that incorporating image-derived indicators related to bench discontinuity conditions into empirical PPV models can improve their fit to the investigated dataset. The inclusion of the image-derived joint factor (JF) in the modified Simangunsong equation enhanced the R^2 value from approximately 0.77–0.81 (for USBM and Sadovsky) to 0.86, confirming the strong influence of discontinuity patterns on vibration attenuation.

The findings of this study highlight that higher JF values—indicating denser jointing and smaller block sizes—correlate with increased vibration attenuation, while lower JF values correspond to conditions with higher PPV. Moreover, image-based discontinuity analysis provides a practical and efficient means for integrating geological variability into blast design and vibration control without extensive field investigation.

In practice, an acceptable PPV threshold can first be defined with reference to relevant international or local vibration guidelines or standards. By doing so, the target value can then be used in the calibrated empirical equations to determine the corresponding maximum allowable charge per delay (Q) for a given set of conditions. That includes rock mass discontinuity characteristics (JF), the distance (R) to the nearest protected structures (e.g., residential buildings), and the selected PPV control criterion. Therefore, blast designers can

subsequently adjust the initiation sequence, delay timing, and the use of decking charges to ensure that ground vibrations remain within the predefined safety thresholds.

It is wished that the results obtained in this study can establish a framework for site-specific vibration assessment that balances simplicity with geological realism, contributing to more efficient, and environmentally compliant quarry operations.

6. Research Limitations and Outlook

This present study has several limitations that should be acknowledged:

1. The vibration data were collected from a thick-bedded marble quarry in eastern Taiwan, and the empirical models were both calibrated and evaluated on this site-specific dataset. As a result, the derived relationships may require recalibration before being applied to other lithologies (e.g., granite or sandstone). Since no external validation or cross-validation procedure was applied, the present results mainly reflect in-sample model performance. Also, the reported performance indicators mainly describe in-sample goodness-of-fit and may overestimate true predictive performance on unseen blasting scenarios. Future work should therefore test the generalizability of the proposed formulation using independent datasets or leave-one-blast-out validation schemes, as well as include applications in different geological settings to more rigorously assess and generalize the models' predictive capability.
2. Although the JF index captures the combined effects of median (D_{50}) and maximum (D_{100}) particle sizes, it remains a simplified indicator of discontinuity and fragmentation conditions. The construction of JF is based on discretizing continuous D50 and D100 values into a small number of classes using engineering judgement. Therefore, the resulting thresholds are somewhat subjective and not necessarily unique or optimal. Parameters such as joint orientation, persistence, spacing, and the presence of infilling materials were also not explicitly considered.
3. In addition, the statistical analysis treated the 106 PPV records as individual observations, although they were derived from 53 blasts with two monitoring points per event. This data structure may introduce intra-blast correlation, so the reported fitting performance should be regarded as indicative rather than fully independent. Future studies should address this issue using blast-level aggregation, clustered error structures, or mixed-effects/hierarchical models.

In light of these limitations, future research should extend the proposed approach to various rock types and geological settings to verify the general applicability of the JF in empirical PPV models. Incorporating additional structural parameters such as joint strike, dip, and spacing, as well as detailed characterization of weak interlayers, may further refine the representation of discontinuity effects. Moreover, vibration frequency should be considered in parallel with PPV, since frequency content strongly influences the dynamic response of nearby structures and the potential for resonance with their natural frequencies. Finally, integrating empirical equations with numerical simulations (e.g., finite element or discrete element methods) may yield more physically based yet practical tools for blast design optimization and vibration control in quarry operations.

Author Contributions: Conceptualization, C.-H.W. and Y.-C.D.; methodology, C.-H.W. and F.-H.L.; software, F.-H.L.; validation, C.-H.W.; formal analysis, C.-H.W. and Y.-C.D.; investigation, F.-H.L.; resources, Y.-C.D.; data curation, F.-H.L.; writing—original draft preparation, C.-H.W.; writing—review and editing, Y.-C.D.; visualization, F.-H.L.; supervision, Y.-C.D.; project administration, C.-H.W.; funding acquisition, C.-H.W. All authors have read and agreed to the published version of the manuscript.

Funding: This research received no external funding.

Institutional Review Board Statement: Not applicable.

Informed Consent Statement: Not applicable.

Data Availability Statement: The original contributions presented in this study are included in the article. Further inquiries can be directed to the corresponding author.

Conflicts of Interest: Author Fu-Hao Lee was employed by the company Taiwan Cement Corporation. The remaining authors declare that the research was conducted in the absence of any commercial or financial relationships that could be construed as a potential conflict of interest.

References

1. Tao, M.; Zhang, X.; Li, Y.; Wang, H.; Chen, J. A Fast Recognition Method for Dynamic Blasting Fragmentation Based on YOLOv8 and Binocular Vision. *Appl. Sci.* **2025**, *15*, 6411. [CrossRef]
2. Yaghoobi, H.; Mansouri, H.; Ebrahimi Farsangi, M.A.; Nezamabadi-Pour, H. Determining the fragmented rock size distribution using textural feature extraction of images. *Powder Technol.* **2019**, *342*, 630–641. [CrossRef]
3. Manzoor, S.; Liaghat, S.; Gustafson, A.; Johansson, D.; Schunnesson, H. Establishing relationships between structural data from close-range terrestrial digital photogrammetry and measurement while drilling data. *Eng. Geol.* **2020**, *267*, 105480. [CrossRef]
4. Nicholls, H.R.; Johnson, C.F.; Duvall, W.I. *Blasting Vibrations and Their Effects on Structures*; U.S. Bureau of Mines Bulletin 656; U.S. Department of the Interior, Bureau of Mines: Washington, DC, USA, 1971.
5. Simangunsong, G.M.; Wahyudi, S. Effect of Bedding Plane on Prediction of Blast-Induced Ground Vibration in Open-Pit Coal Mines. *Int. J. Rock Mech. Min. Sci.* **2015**, *79*, 1–8. [CrossRef]
6. Sadovsky, M.A. The Seismic Effect of Explosions. In *Proceedings of the All-Union Conference on Explosives*; Gostoptekhizdat: Moscow, Russia, 1940; pp. 290–319.
7. Aloui, M.; Abbes, C. Fracturing Influence on the Propagation of the Blast-Induced Ground Vibrations: A Case Study. *Geotec. Geol. Eng.* **2019**, *37*, 5327–5339. [CrossRef]
8. Njock, M.C.; Meli'i, J.L.; Poufonne, Y.K.; Ngnotué, T.; Ndzié, J.P. Influence of Natural Discontinuities and Mechanical Properties on the Fragmentation of Marble by Blasting in Central Africa. *Environ. Earth Sci.* **2021**, *80*, 616. [CrossRef]
9. Ding, X.; Yang, Y.; Zhou, W.; An, W.; Li, J.; Ebelia, M. The Law of Blast Stress Wave Propagation and Fracture Development in Soft and Hard Composite Rock. *Sci. Rep.* **2022**, *12*, 17120. [CrossRef] [PubMed]
10. Huang, X.; Qiu, S.; Liu, Y.; Zhang, B.; Xu, H.; Xu, L.; Li, N. Stress Wave Propagation through Rock Joints Filled with Viscoelastic Medium Considering Different Water Contents. *Appl. Sci.* **2020**, *10*, 4797. [CrossRef]
11. Worsey, P.N.; Farmer, I.W.; Matheson, G.D. The Mechanics of Pre-Splitting in Discontinuous Rock. In *Proceedings of the 22nd U.S. Symposium on Rock Mechanics (USRMS), Cambridge, MA, USA, 29 June–2 July 1981*; Massachusetts Institute of Technology: Cambridge, MA, USA, 1981; pp. 205–210.
12. Zhang, P.; Bai, R.; Sun, X.; Wang, T.; Fei, H.; Bao, S.; Hu, G. Investigation of Rock Joint and Fracture Influence on Delayed Blasting Performance. *Appl. Sci.* **2023**, *13*, 10275. [CrossRef]
13. Deng, Z.; Wang, S.; Wei, T.; Deng, Y.; Ni, J.; Liu, X.; Zhang, Y. Physical Modelling of Propagation Characteristics of Blasting Stress Waves in Rock Masses with Parallel and X-Shaped Intersecting Joints. *Sci. Rep.* **2025**, *15*, 41607. [CrossRef] [PubMed]
14. Hustrulid, W. *Blasting Principles for Open Pit Mining, Volume 1: General Design Concepts*; A.A. Balkema: Rotterdam, The Netherlands, 1999.
15. Singh, P.K.; Roy, M.P.; Paswan, R.K.; Sarim, M.; Kumar, S.; Jha, R.R. Rock Fragmentation Control in Opencast Blasting. *J. Rock Mech. Geotech. Eng.* **2016**, *8*, 225–237. [CrossRef]
16. Wei, D.; Yang, X.; Wang, Y.; Zhang, Z.; Wang, Y. Failure Mechanism of Back-Break in Bench Blasting of Thin Terrane. *Appl. Sci.* **2021**, *11*, 2577. [CrossRef]
17. Lyana, K.N.; Hareyani, Z.; Ariffin, K.S.; Mohd Hazizan, M.H. Effect of Geological Condition on Degree of Fragmentation in a Simpang Pulai Marble Quarry. *Procedia Chem.* **2016**, *19*, 694–701. [CrossRef]
18. Ak, H.; Konuk, A. The effect of discontinuity frequency on ground vibrations produced from bench blasting: A case study. *Soil Dyn. Earthq. Eng.* **2008**, *28*, 686–694. [CrossRef]
19. Campilongo, G.; Ponte, M.; Muto, F.; Critelli, S.; Catanzariti, F.; Milone, D. Geomechanics and Geology of Marine Terraces of the Crotone Basin, Calabria (Italy). *Geosciences* **2024**, *14*, 215. [CrossRef]

Disclaimer/Publisher's Note: The statements, opinions and data contained in all publications are solely those of the individual author(s) and contributor(s) and not of MDPI and/or the editor(s). MDPI and/or the editor(s) disclaim responsibility for any injury to people or property resulting from any ideas, methods, instructions or products referred to in the content.